# Defect-induced Burstein-Moss shift in reduced V_{2}O_{5} nanostructures

Qi Wang, Mathew Brier, Siddharth Joshi, Ajinkya Puntambekar, and Vidhya Chakrapani

Phys. Rev. B **94**, 245305 — Published 13 December 2016

DOI: 10.1103/PhysRevB.94.245305

# Defect Induced Burstein-Moss Shift in reduced $V_2O_5$ Nanostructures

Qi Wang,[a] Mathew Brier,[a] Siddharth Joshi,[a] Ajinkya Puntambekar, and Vidhya Chakrapani,[a,$,#]

[a] Howard P. Isermann Department of Chemical and Biological Engineering

[$] Department of Physics, Applied Physics, and Astronomy

Rensselaer Polytechnic Institute, Troy, NY-12180

[#] Email: chakrv@rpi.edu

ABSTRACT

The main effects of oxygen vacancy defects on the electronic and optical properties of $V_2O_5$ nanowires were studied through *in-situ* Raman, photoluminescence, absorption, and photoemission spectroscopy. Both thermal reduction and electrochemical reduction via lithium insertion leads to the creation of oxygen vacancy defects in the crystal that gives rise to new electronic mid-gap defect states at energy 0.75 eV below the conduction band edge. The defect formation results in delocalization and injection of excess electrons into the conduction band, as opposed to localized electron injection as previously suggested. Contrary to what is seen in most oxides, the presence of vacancy defects leads to band filling and an increase in the optical band gap of $V_2O_5$ from 1.95 eV to 2.45 eV, which is attributed to the Burstein-Moss effect. Other observed changes in the optical properties are correlated to the changes in the electronic structure of the oxide as result of defect formation. Further, *in-situ* Raman measurements during the electrochemical reduction at room temperature show that the oxygen atom that is most readily reduced is the three-fold coordinated oxygen (O3).

Among the various transition metal oxides (TMOs), oxides of vanadium, especially vanadium pentoxide ($V_2O_5$), are unique for several reasons: i) $V_2O_5$ is one of the most easily reduced transition metal oxide with vanadium existing in variety of oxidation states in its various reduced phases, such as $V^{+2}$ as in VO, $V^{+3}$ in $V_2O_3$, or $V^{+4}$ in $VO_2$. Hence, they are widely used as amphoteric catalysts[1,2] for many industrial reactions, such as selective oxidation and reduction of hydrocarbons, oxidation of $SO_2$ to $SO_3$, selective reduction of nitric oxide and many others, in addition to being an effective photocatalyst,[3] ii) the highly layered orthorhombic structure of $V_2O_5$ with a weak van der Waals interaction between layers makes it valuable for monolayer devices[4] and host electrodes for ion intercalation in batteries,[5] sensors[6] and smart materials.[7] In most of these applications, $V_2O_5$ undergoes reduction as a result of formation of oxygen vacancy, $V_O$, defects. It is these defects which impact many of the functional properties characteristic of the oxide, such as enhancement of catalytic activity by acting as hot-spots for adsorptive binding of chemical species,[8] or by impacting electronic properties that result in metal-to-insulator transitions.[9] Thus, understanding the effects of $V_O$ on the electronic properties is important for elucidating the structure-property-function of metal oxides.

Reduction of $V_2O_5$ through the formation of oxygen vacancy, $V_O$, defects have been studied both by theoretical and experimental studies.[10,11,12,13,14,15] It is generally known that the presence of $V_O$ defects causes a change in the oxidation state of neighboring vanadium atoms from $V^{+5}$ to $V^{+4}$ or lower states.[16] In addition, ultraviolet photoemission spectroscopy (UPS) studies show the formation of new mid-gap states as a result of reduction based on the appearance of a board peak centered at 1.3 eV above valence band (VB) edge.[17,15] Some disparity exists in the results of theoretical calculations of reduced oxide. Density functional theory (DFT) cluster work of Hermann *et al.*[18] reported the reduction of neighboring vanadium

atoms that led to increased V 3d orbital occupation. No distinct peaks related to $V_O$ defects in the band gap were reported. Gradient-corrected DFT+U calculations of Scanlon *et al.*[11] showed the creation of new gap states 0.7−1.0 eV above valence band edge for various oxygen vacancy defects. These reports do not indicate any shift in the band gap of reduced $V_2O_5$ or band filling. It was suggested that $V_O$ defects result in increase in electron concentration that is localized on vanadium atoms in the vicinity of the vacancy. Separately, the nature of oxygen vacancy *i.e.* the oxygen that is most readily lost during catalytic reduction has been well studied and debated. [8,11,18,19] The primitive cell of orthorhombic $V_2O_5$ consists of three crystallographically distinct oxygen atoms: the singly-coordinated oxygen (O1) atom which forms vanadyl group V=O, and double- or triple-coordinated bridging oxygen atoms (O2 and O3 respectively). Though there is no clear consensus, it has been generally believed that it is O1 oxygen atom that is most readily lost and thus most important for the catalytic reactions.[11,14]

On the other hand, the effects of electrochemical reduction of $V_2O_5$ by $Li^+$ intercalation have been well studied from the perspective of electrochromic devices.[20,21] $V_2O_5$ is known to exhibit double electrochromic effect, wherein intercalation of $Li^+$ ions is known to cause a decrease in the absorbance in UV spectral region with a shift in the optical absorbance edge and an increase in absorbance in the NIR region. [20,21,] The blue-shift of the absorption edge was attributed to Burstein-Moss effect occurring as a result of band filling. It has been generally accepted that rise in the NIR absorbance in lithiated oxide is due to the absorption by polarons,[20] though photoelectron spectroscopy studies show that appearance of a peak in the UPS spectrum[22] at ~1.1 eV above the valence band maximum and electron paramagnetic resonance studies[12] suggest the vacancy defects may be responsible for NIR absorption. Electron nuclear double resonance by Pecuenard *et al.*[23] suggest that polarons including bound ones trapped on four

vanadium sites around the $Li^+$ ions and free polarons around a single vanadium site give rise to NIR absorption. Theoretical work of Jiang *et al.*[24] on the other hand have predicted metallic conductivity for $Li_xV_2O_5$ even for small values of *x* and attribute the absorbance to free carrier absorption.

In this work, we address some of the key unanswered questions regarding the correlation between optical properties and electronic structure of $V_2O_5$ reduced by two methods: thermal reduction and electrochemical reduction with $Li^+$. We show that both processes result in the generation of high density of $V_O$ defect-related electronic states ~0.75 eV below the conduction band edge and with a corresponding increase in the optical band gap as a result of defect-induced Burstein-Moss shift, which is in contrast to what is seen in most oxides of transition metal including vanadium. As a general trend, the band gap of oxide decreases with increasing oxygen vacancy or reduction, which is evident in the various reduced phases of vanadium oxide whose band gap narrows from 2.0 eV seen in $V_2O_5$ to 0.7 eV in $VO_2$ to 0.4 eV in $V_2O_3$ and no gap in VO.[13,25] The rise of absorbance in the NIR spectral range in reduced oxide is a result of optical excitation of $V_O$ defect related mid-gap states. In addition, using *in-situ* Raman measurements during reduction process, we show that the oxygen atom that most readily participates during electrochemical reduction at room-temperature and gets reduced is the three-fold coordinated oxygen (O3).

Vacancies in vanadium oxide have been probed using a variety of spectroscopic techniques, such as scanning tunneling microscopy,[9,26,27] electron energy loss spectroscopy,[28,29] electron paramagnetic resonance studies,[16,12,23] X-ray absorption measurements,[30] and X-ray photoemission spectroscopy (XPS).[15,17] However, most of these techniques either require ultra-high vacuum (UHV) or controlled environment for operation that makes it difficult to adapt it to

*in-situ* catalytic studies. Here, we use near-infrared photoluminescence (NIR-PL) and Raman spectroscopy that allows for study of vacancy defects and their interaction with redox species under in-operando electrochemical conditions at room temperature, as shown in our recent study.[31] The spectral range of various types of electronic transitions in $V_2O_5$ is shown in Fig.1A. Representative PL spectra of stoichiometric and non-stoichiometric $V_2O_5$ are shown in Fig.1B. The optical gap of nominally undoped $V_2O_5$ is in the range of 1.9-2.5 eV and hence emission spectrum lies in the ultraviolet-to-visible part of the spectral range. In most TMOs, deviation from stoichiometry is a result of the presence of high density of either cationic or anionic vacancies in the lattice. The presence of vacancy defect gives rise to additional electronic states within the band gap. In general, both types of vacancies upon optical excitation gives rise to radiative emissions that lie in the near infrared region of the spectrum. This NIR emission provides a direct tool for probing vacancy formation or passivation by adsorbates or redox species. $V_2O_5$ being one of the most easily reducible oxide and has the propensity to form oxygen vacancy, $V_O$, defects, which can render the crystal non-stoichiometric. From the PL spectra in the NIR spectral region shown in Fig.1B, the presence of $V_O$ defects causes a NIR emission whose peak intensity is centered at 0.75 eV, while fully oxidized $V_2O_5$ shows no NIR radiative emission. In the present work, we show with the combination of both UV-to-NIR PL and absorption spectroscopy that the formation of anionic defects by both thermal and electrochemical reduction leads to Burstein-Moss shift in the optical band gap of the $V_2O_5$.

Vanadium oxide nanowires of varying stoichiometry were prepared by hot filament chemical vapor deposition (HFCVD) technique, which is described in detail in the Methods section. Nanowires with a range of vanadium-to-oxygen ratio were prepared with high purity without the introduction of extraneous reducing agents by simply tuning the filament power and

partial pressure of oxygen and water vapor in the chamber, as was shown in our recent work for other oxides.[32,33] Figure 1C shows the scanning electron micrograph (SEM) of as-synthesized oxide grown on fluorinated tin oxide (FTO) substrates. From the image, the as-synthesized deposits are seen to be vertically- aligned, single crystalline nanowires with diameters in the range of 60-80 nm and length extending to 1-2 microns. As is common in most TMOs, the color of the sample provides a visual measure of the extent of deviation from stoichiometry.[32] In vanadium oxide, fully stoichiometric phase ($V_2O_5$) is orange in optical coloration, while increasing oxygen deficiency shifts the sample color sequentially from orange to yellow-brown to dark green to grayish-black seen in the highly reduced, $V_2O_{5-x}$, phase. Six samples, referred to as S1 to S6 in the text, were prepared with increasing oxygen deficiency, consisting of stoichiometric $V_2O_5$ (orange, Sample S1) to highly reduced $V_2O_{5-x}$ phase (yellow to black, Samples S2 to S6). Optical images of these six samples are shown in the Inset of Fig.1C. Figure 1D shows an optical image and the corresponding NIR-PL map taken at emission energy of 0.75 eV of an oxide surface consisting of $V_2O_5$ and $V_2O_{5-x}$ phase excited using a sub-band gap light of 633 nm wavelength. The stoichiometric phase is orange in optical coloration with no detectable NIR emission, while increasing non-stoichiometric phases shows dark brown coloration and a strong NIR emission due to the presence of $V_O$ defects.

Electrochemical reduction of stoichiometric $V_2O_5$ was performed in a three-electrode cell with application of a negative bias *w.r.t* to a $Li/Li^+$ reference and counter electrode in an electrolyte containing 0.1M $LiClO_4$ in propylene carbonate. The $Li^+$ intercalation into $V_2O_5$ results in a multi-step reduction and phase transformation, which has been studied in detail before.[20] Figure 2A shows the cyclic voltammograms taken at a slow scan rate of 0.5 mV/s of stoichiometric $V_2O_5$ during the first electrochemical reduction-oxidation cycle with a sequential

formation of various $V_2O_5$ phases (also known as bronzes) due to $Li^+$ intercalation. Sharps peaks in the voltammogram seen at various potentials are indicative of phase transformation to various phases, and are similar to the ones reported in the literature.[20] For example, the peak in the current density seen at 3.1 V vs. Li/$Li^+$ is result of phase transformation from α-$V_2O_5$ to ε-$Li_{0.5}V_2O_5$. Progressive insertion of $Li^+$ leads to the formation of δ-$LiV_2O_5$ and γ-$Li_2V_2O_5$ phases, which occurs at a potential of around 2.3 V and 2.0 V vs. Li/$Li^+$ respectively. Further intercalation results in the formation of ω-$Li_3V_2O_5$ at 1.6 V vs. Li/$Li^+$. The formation of γ-$Li_2V_2O_5$ and lower phases at potentials below 2 V are irreversible due to the structural changes that the lattice has to undergo in order to accommodate more than two lithium atoms per unit cell. Structural and electronic shifts caused by $Li^+$ insertion at various electrochemical potential was probed by *in-situ* Raman-PL, *ex-situ* XPS, and absorption measurements in the UV-to-NIR spectral range. All electrochemical potential mentioned in the text are with respect to the reference potential of Li/$Li^+$ that has a standard electrode potential of -3.05 V versus standard hydrogen electrode.[34] In addition to nanowire samples, experiments were also repeated with commercially available micron-sized powders of $V_2O_5$. No major differences in the results were seen between nanowires and microparticles.

Crystalline $V_2O_5$ forms an orthorhombic layered structure along the *c* axis of the unit cell and belongs to the space group of *Pmmn* (a = 11.510 Å, b = 4.369 Å, c = 3.563 Å). The primitive cell contains four V atoms and ten O atoms that correspond to two stoichiometric $V_2O_5$ units. Each layer consists of a periodic arrangement of edge-sharing and corner-sharing distorted trigonal $VO_5$ pyramids and the layers are held together by weak vanadium-oxygen van der Waals interactions. Three different types of oxygen bonding exist within the $V_2O_5$ structure: terminal vanadyl oxygen (V=O1), double bridging oxygen to two vanadium sites, and triple bridging

oxygen.[11] The nearest neighbors of each vanadium atom form a distorted octahedron in which one vanadyl-oxygen bond (V=O1), oriented perpendicular to the (001) plane, is unusually short (1.58 Å), and another that consists of vanadium bonded to an oxygen atom in an adjacent layer is unusually long (2.79 Å). The bridging oxygen (denoted as O2) connects two adjacent vanadium atoms with two V−O bond lengths of 1.77 Å, and three-fold coordinated oxygen (denoted as O3) with three V−O bond lengths of 1.88, 1.88, and 2.02 Å.[35] Figure S1 in the Supplementary Information[36] shows the schematic of co-ordination of vanadium ion in $V_2O_5$.

$V_2O_5$ is a very effective catalyst for many important reactions because of the ease with which it loses the lattice oxygen in many oxidative reactions. The resulting oxygen vacancies, associated with the three distinct lattice oxygen atoms, play a crucial role in catalytic reaction by acting as hot spots for adsorptive binding of reacting species. Several detailed studies have been undertaken using various theoretical and spectroscopic tools to elucidate the nature of oxygen that most readily participates in catalytic reactions.[19,11,16,37,38] However, there is no clear consensus yet on the results of these studies. The computed theoretical density of states (DOS) by DFT calculations, which are in agreement with the results from angle-resolved ultraviolet photoemission spectroscopy (ARUPS), show that the three differently coordinated oxygen atoms contribute to different region of the valence band states.[39] DOS contributed by terminal vanadyl oxygen (O1) are localized near the center of the valence band, whereas those of two- and three-fold bridging oxygen (O2 and O3) yield a broad distribution spanning the full width of valence band and peaking near the periphery. ARUPS results of Hermann *et al*.[18] on the reaction of $V_2O_5$ (010) with hydrogen showed that hydrogen affected peripheral valence band DOS more than the states from central region. Hence, they concluded that bridging oxygen atoms (O2 and O3) most readily react with adsorbed $H_2$ to create oxygen vacancies as these oxygen atoms are

more weakly bound to the surface than terminal oxygen (O1). A similar conclusion was drawn from the IR spectroscopic results of Ramirez *et al.*[19] on that relative changes in the intensity of vibration stretches corresponding to O3 and O2 compared to the O1 stretch of $V_2O_5$ during reaction with dimethyl sulfoxide at 123 ºC. In both these studies, distinction could not be made between the reactivity of O2 and O3 bridging oxygen atoms. Similarly, Tepper *et al.*[40] studied the reactivity of unsupported $V_2O_5$ surface towards atomic hydrogen through HREELS and ARUPS techniques and concluded that the most reactive oxygen atom is the bridging oxygen, while terminal and three-fold coordinated sites are stable with respected to the interaction of atomic hydrogen. In contradiction to these results, both prior[14,41,42] and recent[11] theoretical calculations by several researchers noted that the formation energy of O1 vacancy is the lowest compared to O2 and O3 vacancies based on gradient-corrected DFT+U results and concluded that O1 vacancy is the most stable defect, and thus the most likely to be active during reduction reaction. Further UPS results of Wu *et al.*[17] during thermal reduction of $V_2O_5$ showed a decrease in the intensity of both central and top region of VB during reduction in contradiction to the results of Hermann and coworkers. Studies by Ozkan *et al.*[42] on the reducibility of $V_2O_5$ with $H_2$ and $NH_3$ by temperature programmed desorption also showed that the interaction of reducing agents occurs primarily with the terminal vanadyl (O1) oxygen atom. In all, significant disparity exists in the results reported in the literature to conclusively assign the nature of O vacancy. In addition to the above reports, significant number of in-depth catalytic studies has been performed on supported $V_2O_5$. The effect of support is also of great importance because of the presence of reactive sites at the interface of oxide and support;[43,44,45,46,47] hence the results from supported catalysts cannot be extended to unsupported $V_2O_5$ catalyst.

In the present work, we use Raman spectroscopy to study the relative reactivity of the three different lattice oxygen atoms towards $Li^+$ ions to identify the one that is most readily reduced electrochemically at room-temperature. Reaction of $Li^+$ with various lattice oxygen atoms results in the formation of Li–O[48] or $Li_2O$ and a $V_O$ defect. Raman spectroscopy is a powerful and sensitive tool for studying structural and bonding changes occurring in oxide and has been widely used for in-situ gas-phase catalytic studies.[47,45,46,49] The technique can show distinct peaks for the Raman-active bending and stretching modes of the three different V-O bonds, and thus can distinguish between reactivity of various oxygen atoms. Curve 'a' in Fig.2B shows typical Raman spectra of stoichiometric $V_2O_5$. Raman peaks at ν-996 $cm^{-1}$, δ-407 $cm^{-1}$ and δ-285 $cm^{-1}$ correspond to the terminal vanadyl oxygen (V=O1), where 'ν' denotes stretching and 'δ' represents the bending modes of vibration respectively. Peaks at ν-702 $cm^{-1}$ and δ-483 $cm^{-1}$ are assigned to the double-coordinated oxygen (V-O2), and the triple-bridging oxygen can be identified by peaks at ν-528 $cm^{-1}$ and δ-304 $cm^{-1}$. Low frequency peeks located at 103 $cm^{-1}$, 145 $cm^{-1}$ and 198 $cm^{-1}$ correspond to the external vibrational modes. All Raman peaks are in good agreement with previously published data for orthorhombic α-$V_2O_5$.[50,51] Evolution of Raman bands of $V_2O_5$ upon reaction with $Li^+$ at various electrochemical potentials is shown in Fig.S2 in the Supplementary Information. Intensities of all Raman features decrease to various extents with increasing amount of $Li^+$ ions in the lattice, which could be due to several effects. For example, increasing structural disorder could lead to the reduction in the overall intensity of the Raman peaks, which may be especially true at high $Li^+$ concentration in $V_2O_5$. Lithium insertion also leads to changes in the color of $V_2O_5$ samples with strong increase in absorption coefficient at visible and infrared spectral region (Fig.3A) as a result of defect formation that leads to a smaller Raman scattering cross section. Absorption of both the incident and scattered

light by these defects causes a reduction in the sampling depth and, hence, a reduction in the intensity of the Raman signal observed for a given concentration of $V_2O_5$.[52] Curve 'b' in Fig.2B represents the Raman spectra taken at a potential of 3.2 V. The comparative changes in the intensity of stretching modes of each of three V−O bonds as a result of reaction with $Li^+$ is summarized inn Table S1 in the Supplementary Information. Comparison of curve 'b' to curve 'a' shows that the intensity of Raman peaks at 528 $cm^{-1}$, which corresponds to vanadium bonded to three-fold coordinated oxygen (O3), changed 10% due to reaction with $Li^+$, whereas the characteristic bands of double-coordinated bridging oxygen, V-O2 changed 2% while the vanadyl oxygen (V=O1) remains practically unaltered with only 0.5% change. The rapid decrease in the band intensity of V−O3 over V=O1 indicates that the O3 is the oxygen atom that most readily participates in the oxidation reaction with $Li^+$ to form $Li_2O$. Both theoretical[11,41] and experimental reports[16,53] on the gas-phase catalytic studies in the literature allude to vanadyl oxygen, V=O(1) as being the most active during catalytic reactions at high temperature. Our results on the other hand indicate that vacancies associated with O(3) are the ones most readily formed under electrochemical conditions at room temperature, which is inline with the IR spectroscopic results of Ramirez *et al.*,[19] and thus are most likely to play an important role in many catalytic reactions over $V_2O_5$ surfaces. It must be stressed that $Li^+$ insertion into $V_2O_5$ leads to structural distortions that result in complex phase transformations (α-, ε-, δ-, γ- $Li_xV_2O_5$) that have varying electronic structures and hence vibrational dynamics. Recently, Smirnov *et al.*[54] studied the structure, electronic states, and vibrational dynamics of γ-$LiV_2O_5$ by combined use of quantum-chemical calculations and Raman spectroscopy, and showed the lengthening of the vanadyl V−O1 bonds in the lithiated structure. The phase transformation due to Li intercalation was shown to significantly change the Raman spectrum that included formation of

new intense Raman peaks at 737 and 462 $cm^{-1}$ resulting from increase of asymmetry of the V−O3−V bridges that leads to the transformation of the asymmetric and symmetric V−O3−V vibrations into V−O3 bond stretching vibrations. These results show that straight-forward comparative analysis of Raman spectrum of pristine and lithiated $V_2O_5$ is inaccurate. In the present study however, comparison of Raman intensities of various V-O bonds was done between pristine $V_2O_5$ and $V_2O_5$ reduced at 3.2 V vs. $Li/Li^+$. Though the formation of ε-$LiV_2O_5$ occurs at ~3.1 V, the lithiated phases of $LiV_2O_5$ (α, ε, δ) at low $Li^+$ concentration (or high voltages) are structurally very similar to the α-$V_2O_5$ polymorph. The changes in the V-O bond lengths at such low $Li^+$ concentration is minimal, as evidenced by the absence of frequency shifts in the various V-O stretching vibrations seen in the two spectra. Hence, we believe that the Raman scattering cross-section in both cases is nearly the same (minimal changes in absorption coefficient), as evidenced by the similar band widths and shapes. However, this assumption fails at higher $Li^+$ loading in $V_2O_5$, where dramatic decreases in the intensity of Raman signals were observed.

Injection of $Li^+$ and $e^-$ into metal oxide during electrochemical reduction results in the formation of LiO or $Li_2O$, [55,5,48] as observed previously by both in-situ transmission electron microscopy[56] and ex-situ XRD measurements,[57] and was confirmed in the present study by XPS. The XPS spectrum of Li 1s peak at the binding energy of 55.5 eV corresponds to $Li_2O$ and is shown in Fig.S3 in the Supplementary Information. The formation of the $Li_2O$ results in a $V_O$ defect and decrease in the oxidation state of $V^{+5}$ to $V^{+4}$ or lower states that was also monitored via XPS. The change in the valence state is a result of charge transfer from the defect to the neighboring vanadium atoms. The XPS spectra of V 2p core level emission peaks of stoichiometric (curve a) and lithiated phases (curves b & c) of $V_2O_5$, biased at potentials of 3.2

and 2.5 V, is shown in Fig.2C. The binding energies of the V 2p levels are 516.9 and 524.5 eV for V $2p_{3/2}$ and V $2p_{1/2}$, respectively, and that of the O 1s level is 529.6 eV (not shown). With increasing lithiation, the spectra (b & c) show the broadening of V $2p_{3/2}$ and V $2p_{1/2}$ peaks and a shift to lower binding energy. In addition, a new shoulder peak at binding energy of 515.8 eV appears on the low binding energy side of V $2p_{3/2}$, which corresponds to $V^{+4}$, and whose intensity increases with increasing $Li^+$ in the crystal. The decrease in the binding energy of the core level (chemical shift) indicates a decrease in the positive charge of vanadium atom. The presence of $V_O$ defects gives rise to new electronic states within the band gap that is was evident both from the VB spectra at lower binding energy (shown in Fig.2D) that shows the appearance of a broad peak centered at 1.3 eV above VB edge in lithiated sample (curves b & c) and the NIR PL emission results (Fig.3D) that is discussed later.

The spectral absorption properties of pristine and lithiated $V_2O_5$ nanowires were measured *ex-situ* in the wavelength range of 300-2600 nm in diffuse reflectance mode with $BaSO_4$ powder as the reference. The nanowire powder was scraped from the FTO substrate post lithiation and deposited on $BaSO_4$ pellet for diffuse reflectance measurements. Care was taken to minimize air exposure before measurements. To elucidate the effects of band gap shifts with $Li^+$ insertion, spectra were corrected for baseline absorbance and normalized to the peak absorbance value. The normalized absorbance spectrum recorded after electrochemical reduction at various potentials *w.r.t* $Li/Li^+$ is shown in Fig.3A. The absorbance of the pristine sample increases monotonically with decreasing wavelength from $\lambda$=570 nm, which is consistent with the transition across the indirect band gap of 1.95 eV between R to $\Gamma$ symmetry points in the Brillouin zone.[35] Lithiated $V_2O_5$ shows absorption peaks both in the visible as well as NIR region. With progressive $Li^+$ intercalation, the optical absorption edge in the short wavelength

region shifts from λ=570 nm under no bias to λ=495 nm when biased to 1.5 V vs. $Li/Li^+$. The values of band gap estimated from the Tauc plot (See Fig.3B) shows a corresponding increase from 2.10 eV to 2.45 eV. In addition to the changes in the absorbance in the short wavelength region, the absorbance in the NIR region also increased with increasing $Li^+$ intercalation. The unbiased sample showed no NIR absorbance, while sample biased at negative potential showed an NIR absorption peak in the spectral range of 1000-1500 nm. With increasing $Li^+$ concentration, not only does the peak intensity of NIR absorbance increase, but also the peak position shifts to shorter wavelength, i.e. from λ=1500 nm under no bias to λ=1050 nm when biased to 1.5 V vs. $Li/Li^+$. These changes in the both band gap and NIR absorbance are consistent with the double electrochromic effect of $V_2O_5$ observed by previous researchers,[7,20] wherein the oxide shows anodic electrochromic effect in the near-ultraviolet region, *i.e.* its transmission increases with lithiation, and a cathodic electrochromic effect in the NIR region where its transmittance decreases with lithiation.

Change in the PL emission in the UV-to-NIR spectral region was measured *in-situ* during electrochemical reduction and is shown in Fig.3C and 3D. Spectra in the UV-Vis region were obtained using He-Cd Laser at optical excitation wavelength of λ= 325 nm. As stated earlier, $V_2O_5$ is a easily reducible oxide and irradiation with even moderate energy UV or electron probe beams during measurements can easily cause oxygen desorption from the lattice. To avoid forming $V_O$ defects during PL measurements, spectra in the NIR region were taken using a sub-band gap He-Ne laser at an excitation wavelength of 633 nm. Care was taken to minimize laser heating. As seen from Fig.3C & 3D, stoichiometric $V_2O_5$ shows a PL emission peak at 1.95 eV and no emission in the NIR spectral region. At low concentration of $Li^+$ intercalated into the lattice, such as when the sample is biased to 3.2 V vs. $Li/Li^+$, the intensity of peak PL emission at

1.95 eV increases. However, at potentials more negative than 3.2 V, the peak PL emission shifts to a higher energy centered at 2.45 eV. Concomitantly, a new spectral feature in the NIR range develops whose peak emission lies at energy, E= 0.75 eV. From Fig.3D it can be seen that the intensity of this NIR emission increases with decreasing electrochemical potential, which corresponds to increasing $Li^+$ concentration in $V_2O_5$.

Like electrochemical reduction, thermal reduction of $V_2O_5$ during growth generates $V_O$ defects that have a profound effect on the optical properties, as shown in Fig.4. The concentration of $V_O$ defects determines the stoichiometry and the crystal structure of the reduced phase. All samples, S2 to S6, of reduced oxide showed the characteristic Raman features of either $V_2O_5$ or $V_6O_{13}$ or both, as shown in Fig.3A. Table S2 in the Supplementary Information summarizes the nature of various Raman peak positions for $V_6O_{13}$, $VO_2$ and $V_2O_5$ as given in reference [50]. Note that the vibrational stretches of both $V_6O_{13}$ and $V_2O_5$ occur at nearly same wavenumbers but shifted by value of 8-10 $cm^{-1}$. This similarity in the spectra is due to the similarity of the structural units which form the crystals. Both crystallographic phases consist of layers of $VO_6$ octahedron that are relatively weakly bonded to each other. Comparison of expected peak to the measured Raman peaks in the oxidized and reduced phase indicates that Samples S1, S2 (yellow coloration) and S3 (dark-yellow coloration) were pure phases of $V_2O_5$. Samples S4 (brown coloration) and S5 (dark-green coloration) showed mixed phases of $V_2O_5$ and $V_6O_{13}$. Sample S6 (black coloration) was predominantly $V_6O_{13}$. This was further confirmed by X-ray diffraction (XRD) patterns from the reduced samples (S4 and S6), which is shown in Fig.S4 in the Supplementary Information. The changes in the stoichiometry of the samples as a result of reduction was determined from the background corrected XP spectra of the V $2p_{3/2}$ peak shown in Fig.4B. The removal of the originally negatively charged oxygen ion as neutral species

leads to the transfer of electrons to the neighboring vanadium and changes in the oxidation state of vanadium in the vicinity of the vacancy defect from $V^{+5}$ to $V^{+4}$. The increase in the intensity of $V^{+4}$ binding energy peak is evident in the XPS spectra of reduced samples (S3, S4 & S5) compared to fully oxidized sample (S1) that shows no appreciable signal corresponding to $V^{+4}$. From the ratio of integrated intensity of $V^{+5}$ to $V^{+4}$, the concentration of $V^{+4}$ relative to $V^{+5}$ in the reduced phases was estimated and is summarized in Table S3 in the Supplementary Information. The formation of mid-gap states as a result of $V_O$ was monitored at the low-binding energy valence spectra that are shown in the Figure S5 in the Supplementary Information, which shows the development of new peak at ~1 eV above the valence band maximum in non-stoichiometric samples. The $V_O$ defect-induced changes in the absorbance and PL emission were measured and are shown in Fig 4C-F. Similar to changes induced by $Li^+$, increasing concentration of $V_O$ defects in the crystal causes a blue-shift of the optical absorption edge from 570 to 520 nm along with the increase in the absorbance in the NIR spectral range from 1200 to 1700 nm. From the Tauc plot (Fig.4D), the shift in the band gap was calculated to be from 2.1 to 2.25 eV between sample S1 (orange, $V_2O_5$) and sample S6 (black, $V_2O_{5-x}$). Similarly, the energetic position of band-edge PL emission shifts from 1.95 eV to 2.45 eV between stoichiometric (S1-S3) and reduced oxides (S4, S5 and S6), as shown in Fig.4E. The presence of $V_O$ defects also gives rise to NIR emission peak centered at 0.75 eV, whose intensity increases with increase in concentration of defects.

The changes in the optical properties can be understood by considering the band structure of $V_2O_5$. Like most TMOs, the valence band of $V_2O_5$ is derived primarily from the O 2p orbitals, while the conduction band predominantly shows the metal d-band characteristics.[58,59] However, the complicated layered structure of $V_2O_5$ with distorted octahedrons makes the lattice

effectively two dimensional and gives rise to many bands with low dispersion. In addition, the distortion leads to strong indirect V-V interactions across the intermediate bridging oxygen that links the double V-O chains in the crystal structure. As a result, the bonding part of the d-band is split off from the rest of the d-band and forms an intermediate d-band, referred to as "split-off" band, which lies below the main d-band. Theoretical calculations of Lambert and coworkers[58] on the origin of the split-off band suggests that this band originates from the V $3d_{xy}$ and V $3d_{yz}$ orbitals ($t_{2g}$ symmetry) with very small admixing from O $2p_{x,y}$ orbital. Both absorbance edge seen at 570 nm and the PL emission at 1.95 eV indicate that stoichiometric $V_2O_5$ is a semiconductor with a band gap of 2.0 eV. This optical gap corresponds to the energy difference between the top of the valence band (VB) derived from O 2p band and the lower edge of the split-off V 3d band that forms the conduction band (CB). The Fermi-level in a nominally undoped oxide lies near the lower edge of the split-off band. Optical transitions between the split-off band and the main part of the d-band are parity forbidden. Stoichiometric oxide shows no NIR emission, which indicates that there are no optically measurable defects states within the band gap. The band structure and the various radiative transitions occurring upon optical excitation in both stoichiometric and reduced oxide are shown schematically in Fig.5.

Both thermal and electrochemical reduction processes result in the generation of $V_O$ defects and change in the oxidation state of neighboring $V^{+5}$ atoms to $V^{+4}$ or lower oxidation state. The formation of this defect pair creates additional electronic mid-gap states within the band gap. Electrochemical reduction process results in injection of e− into the CB from the FTO back contact and insertion of $Li^+$ into the lattice. In thermal reduction, the neutral oxygen atoms that are being removed from the crystal donate their excess electrons to the vanadium atoms. Prior studies have indicated that these excess electrons are localized on the vanadium atoms near

the vicinity of defects.[11,39] However, the shift in the optical absorption edge with increasing concentration of $V_O$ defects suggest that the e− are delocalized over the entire crystal and are part of the conduction band electrons. This $e^-$ injection results in the filling of the split-off d-band and shift in the Fermi level to a higher energy. When the concentration of conduction electron, $n_e$, is low, the Fermi level remains within the split-off d-band. The slight increase in the $e^-$ concentration results in the increase in the intensity of band edge PL emission at 1.95 eV, which is seen in both types of reduced oxide. However, with increasing $n_e$ during progressive reduction or $Li^+$ intercalation, the Fermi level abruptly move into the main part of V 3d band upon complete filling of the split-off band. As a result, the optical absorption of the sample shows a shift to a lower wavelength *i.e.* from 570 nm in pristine sample to 495 nm. This optical shift in the absorption edge to higher energy as a result of band-filling is referred to as the Burstein-Moss effect. The optical transitions then occur between the top of the O 2p valence band and the bottom of the main V 3d band. The abrupt shift in the peak position of PL emission from 1.95 eV to 2.45 eV indicates that the energetic position of the split-off band is ~0.5 eV below the main d-band, which is consistent with the results of both theoretical calculation[58] and prior optical absorption studies.[20] As mentioned earlier, this increase in the optical band gap as result of $V_2O_5$ reduction is unexpected because the band gap of most oxide decreases with increasing oxygen vacancy or formation of metal d band DOS within the band gap,[60] including vanadium oxide whose band gap narrows from 2.0 eV to 0.7 eV in $VO_2$ to 0.4 eV in $V_2O_3$ and no gap in VO. The evolution of increasing DOS within the forbidden gap and narrowing of the gap in reduced vanadium oxide has been observed by photoemission studies.[15] Interestingly, thermal reduction in other n-type TMOs, such as $WO_3$ or $MoO_3$, leads to increase in n-type conductivity with e− injection into the conduction band; however, they show no shift in the optical band

gap.[32] The blue-shift seen in $V_2O_5$ may be a consequence of the low dispersion of conduction band states, which leads to band filling even with relatively small concentration of e− injection.

From the energetic position of NIR emission peak of both $V_2O_{5-x}$ and $Li_xV_2O_5$, and from the fact that presence of $V_O$ defects induces n-type conductivity in $V_2O_5$, it can be concluded that $V_O$ defect states are located ~0.75 eV below the split-off d-band, which is consistent with the theoretical predictions of Scanlon *et al*.[11] This band filling causes blue-shift not only of the optical absorption edge but also the peak absorbance seen in the NIR spectral range. Previous studies[20] have attributed this NIR absorption to small polaron absorption and the broadening of this absorption band with lithiation to the lattice disorder that causes electronic transitions to neighboring sites to take place at higher energy. Considering both the NIR PL emission and absorption results seen in the present work, we attribute the NIR absorption to be a result of electronic transition from the $V_O$ defects located 0.75 eV below split-off d-band to the upper part of the main d-band. The observation that NIR absorbance also blue-shifts with increasing electron concentration indicates that this absorbance is a result of electronic excitations involving main d-band states and supports our above conclusion. The NIR PL emission seen at 0.75 eV is a result of electron transitions between the split-off d-band and the $V_O$ defect states.

It can be argued that the changes in the optical gap of $V_2O_5$ seen with lithiation is not a true Burstein-Moss effect, as structural distortions and phase transformations can lead to marked changes in the Mott-Hubbard band. In this case, one can argue that the changes in the observed optical spectra be attributed to the differences in the fundamental energy band gap ($E_{CB}-E_{VB}$) of various lithiated phases, as opposed to the proposed explanation where changes were attributed to the increase in the optical gap ($E_F-E_{VB}$) with a constant energy band gap. It must be pointed out that though $Li^+$ insertion into $V_2O_5$ leads to phase transformations whose structural

parameters maybe markedly different from parent $V_2O_5$, as pointed out by Smirnov *et al*.[54] for γ-$LiV_2O_5$, spin-polarized DFT+U calculations however do not indicate shifts in the fundamental energy gap, and the major effect of lithiation on electronic structure is the formation of midgap states,[54,11,61] as is observed in the present study. The similarly in the changes in the optical properties (optical band gaps increase) between electrochemically and thermally reduced $V_2O_5$, where marked structural phase transformation only occurs in the former case, support the conclusion that the fundamental electronic gap remains nearly the same and the increase in the optical gap is due to Burstein-Moss effect. Finally, Fig.S5 in the SI shows the changes in the optical absorbance spectra as a result of $Li^+$ insertion into a reference n-type sample, tungsten oxide ($WO_3$). While the rise in NIR absorbance peak at ~1200 nm in $Li_xWO_3$, which indicates the formation of $V_O$ defects as a result of $Li^+$ insertion, is similar to that in seen in $Li_xV_2O_5$, however, unlike in $V_2O_5$ that shows Moss-Burstein shift in the optical gap, no blue-shift of the absorption edge is seen in $WO_3$ with $Li^+$ insertion.

In summary, we show here the main effects of oxygen vacancy defects on the electronic and optical properties of $V_2O_5$ nanowires through *in-situ* Raman/PL, absorption, and photoemission spectroscopy. Both thermal and electrochemical reduction of $V_2O_5$ leads to creation of oxygen vacancy defects with the delocalization and injection of excess electrons into the conduction band, as opposed to localized electron injection as previously suggested. Vacancy formation also gives rise to new electronic mid-gap defect states that lie ~0.75 eV below the split-off d band. Band filling with excess electrons leads to Burstein-Moss shift of the optical absorption edge and PL emission from 1.95 eV to 2.45 eV. This increase in the optical band gap is contrary to that seen in most oxides, where reduction leads to decrease in the band gap. Further, *in-situ* Raman measurements during reduction process show that the oxygen atom

that most readily reacts during room-temperature electrochemical reduction is the three-fold coordinated oxygen (O3).

**ACKNOWLEDGEMENTS**

The authors gratefully acknowledge the financial supports of National Science Foundation grant (CBET, Award no: 1511733) and Rensselaer Polytechnic Institute.

Methods and Materials

***Synthesis of $V_2O_5$ nanostructures***: Nanowires of various stoichiometries were synthesized by HFCVD in a custom-built quartz reactor. Detailed description of the reactor and the technique can be found in our previous publication.[32] A 0.5 mm diameter vanadium wire was resistively heated to filament temperatures of 1000-1500K using a variable voltage power supply. The reaction of oxygen with the hot vanadium filament results in the formation of vanadium oxide. Deposition on different substrates was done by placing them approximately 5 mm below the filament during growth. Substrate temperatures during growth were in range of 500-800K. Fluorine-doped tin oxide (FTO) coated glass served as the substrates for most of electrical measurements. Prior to deposition, substrates were cleaned sequentially with soapy water, acetone, ethanol and deionized water, and dried under nitrogen. Deposition was carried out under oxygen or oxygen mixed with humid air at a reactor pressure of 1 torr. Stoichiometry of the oxide was controlled by modulating the total power delivered to the filament and the composition of the gas phase species. Stoichiometric $V_2O_5$ deposit (sample S1) was obtained

under pure oxygen atmosphere. Introduction of humid air into the reactor and higher filament temperature promoted the formation of reduced phases of $V_2O_5$ (Samples S2 to S6).

***Characterization***: The morphology of the samples was examined by SEM (Carl Zeiss SUPRA 55 FESEM). The composition and structure of $V_2O_5$ were characterized by XRD (PANalytical X'Pert Pro Diffractometer) and XPS (Physical Electronics PHI 5000 VersaProbe). XPS measurements were carried out at room temperature in a UHV system with a base pressure of $10^{-9}$ mbar. Al Kα radiation (hν= 1486.6 eV) from a monochromatic X-ray source was used for excitation. The spectra are given in binding energy (BE) referenced to the Fermi level of a sputter cleaned Au reference sample.

*Optical absorption measurements*: Absorbance (A) of the $V_2O_5$ samples were recorded in the diffuse reflectance mode using a UV-Vis-NIR spectrophotometer (Shimadzu UV-3600) in the range of 300-2600 nm. For each measurement, samples were scraped off from the substrate, and then uniformly spread onto a layer of barium sulfate ($BaSO_4$) powder that served as the reflectance standard. The band gap of the material was determined from the Tauc plot, which is given by the relationship:[33]

$$(h\nu\alpha)^{\frac{1}{n}} = B\,(h\nu - E_g)$$

where $h$ is the Planck's constant, $\nu$ is frequency, $\alpha$ is the absorption coefficient, B is a proportionality constant, and $n$ denotes the nature of the allowed transitions, $n = 1/2$ for direct and $n = 2$ for indirect transitions. The optical band gap was estimated by taking the intercept of the extrapolation of the tangent line to the linear portion of the curve to the inflection point of x-axis.

*In-situ Raman and PL measurements* were performed with HORIBA Scientific LabRAM HR Evolution spectrometer. Raman spectra were acquired at room temperature using the 633nm line

of a helium-neon laser at a laser power of 16 mW. Band gap PL measurements in the energy range of 3.8 to 1.2 eV were done using 325nm excitation energy of He-Cd Laser. NIR PL spectra were recorded in the 0.7-1.8 eV range using a liquid nitrogen-cooled InGaAs charge-coupled detector at an excitation wavelength of 633nm. All measurements were done at room temperature. Care was taken to avoid laser heating of the sample. For *in-situ* measurements, a small stainless steel electrochemical cell with a quartz window was constructed.

*Electrochemical studies*: $Li^+$ insertion into $V_2O_5$ was performed in a glove box under argon atmosphere using a standard three-electrode setup that consisted of Li metal (MTI Corp.) as both the counter and reference electrodes. The composition of the electrolyte was 0.1M lithium perchlorate ($LiClO_4$, Aldrich, 99.99%) in anhydrous propylene carbonate (PC, Sigma-Aldrich, 99.7%). The intercalation process was done with application of constant step potential in the range of 3.2-0.5V *vs.* $Li/Li^+$ using a Zahner IM6 electrochemical workstation, and allowed to reach equilibrium that took approximately 3-5hrs. For absorption measurements, samples were emmersed from the electrolyte and dried completely inside the glove box before each run.

FIGURES

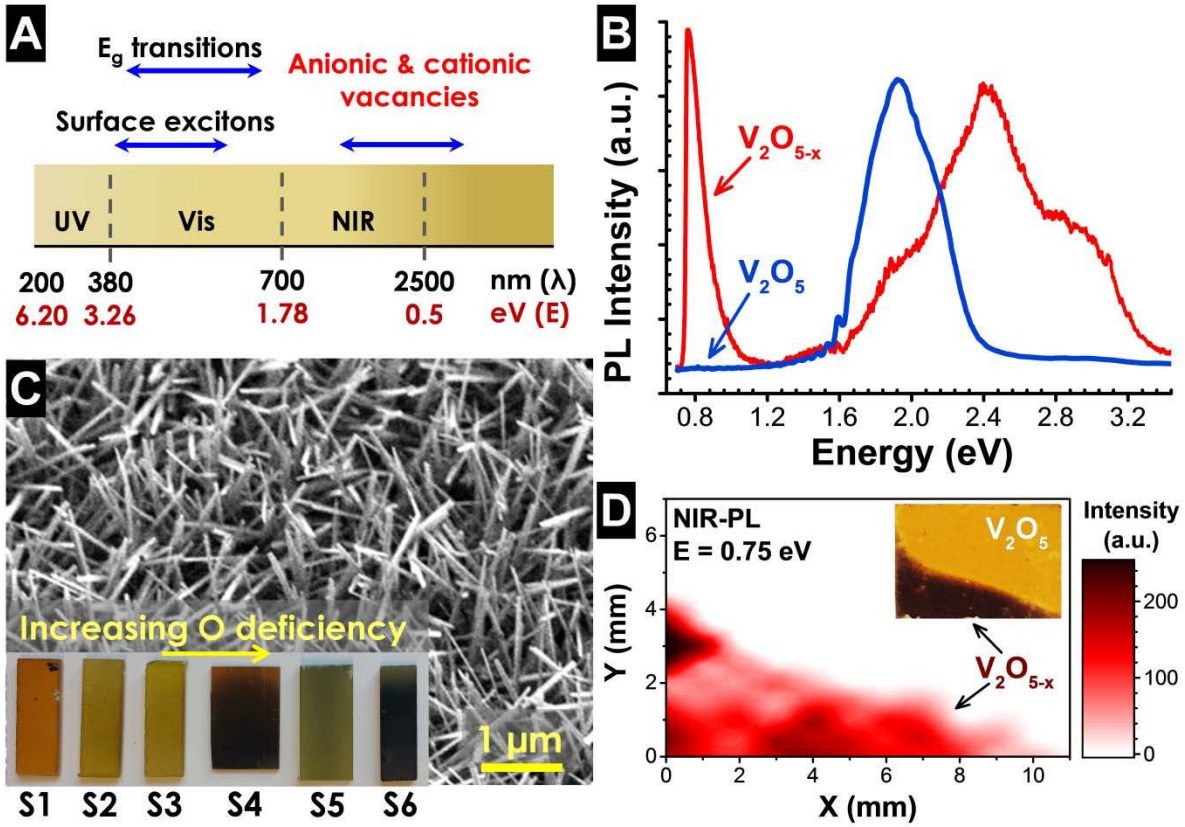


Figure1. A) Energy range of the various radiative transitions in vanadium oxide spanning from UV to NIR spectral region, B) Representative emission spectra of non-stoichiometric vanadium oxide ($V_2O_{5-x}$) and stoichiometric ($V_2O_5$) upon excitations with 633nm and 325 nm lasers in the energy range of 0.7-1.3 eV and 1.3-3.3 eV respectively, C) Scanning electron micrograph image of single crystal $V_2O_5$ nanowires grown on FTO substrates, Inset: Optical images of vanadium oxide samples with increasing oxygen deficiency, D) Optical micrograph and the corresponding NIR PL map taken at emission energy of 0.75 eV of a oxide surface consisting of oxidized ($V_2O_5$) and reduced ($V_2O_{5-x}$) oxide. The region of $V_2O_{5-x}$ containing $V_O$ defects shows a strong NIR emission, while the $V_2O_5$ region shows no detectable NIR emission.

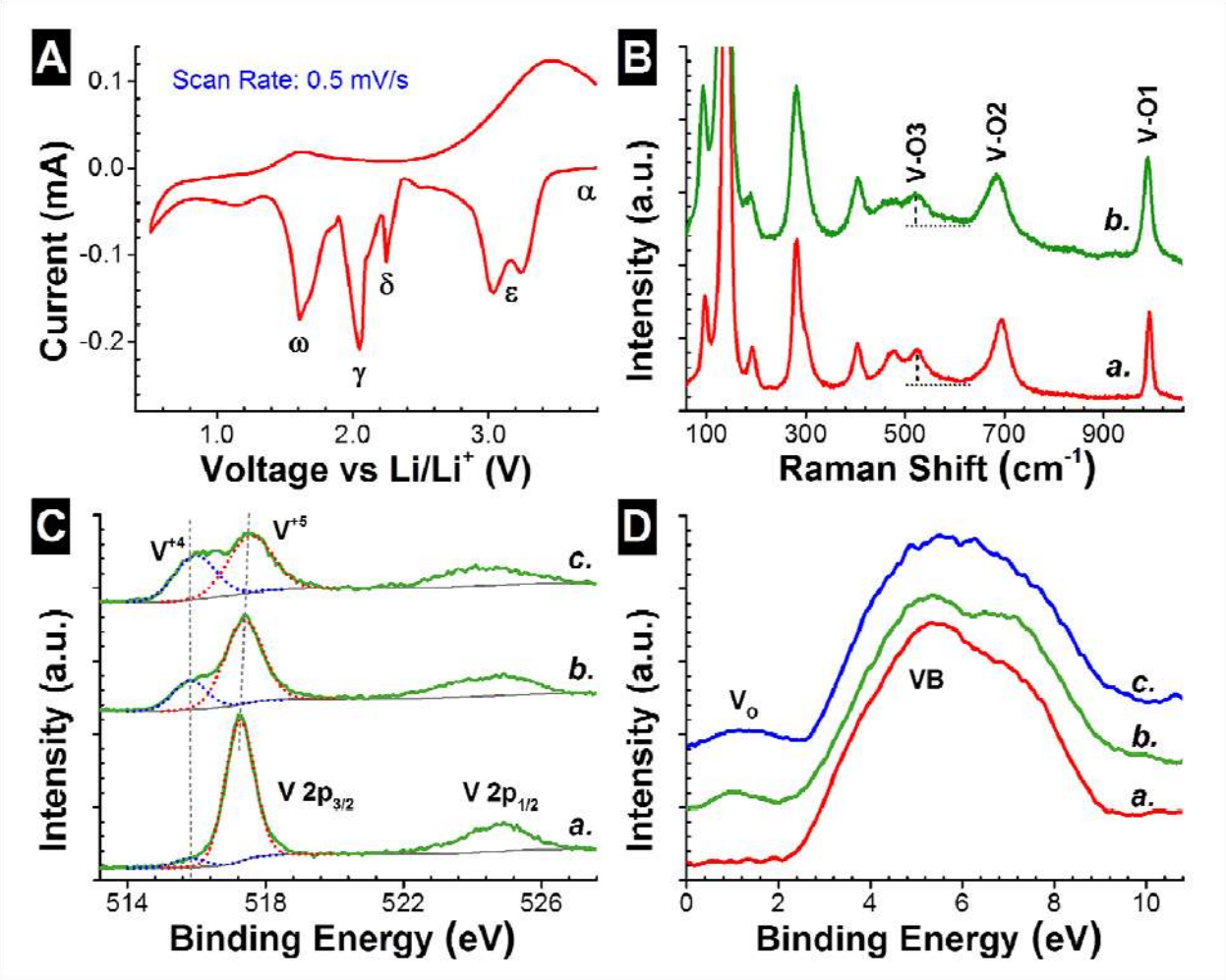


Figure 2 A) Cyclic voltammogram of α-$V_2O_5$ during electrochemical cycling in 0.1M $LiClO_4$ in propylene carbonate taken at a scan rate of 0.5 mV/s. The peaks in the voltammogram correspond to the phase transformation of $V_2O_5$ to various lithiated phases due to $Li^+$ intercalation, B) *in-situ* Raman spectra of $V_2O_5$ at open circuit potential (OCP, curve a) and at potential of 3.2 V vs. $Li/Li^+$ (curve b). Raman peak at 528 $cm^{-1}$ corresponding to the vanadium bonded to bridging oxygen (O3) shows the largest decrease in the intensity, which suggests that O3 oxygen is the most easily reduced, C) XPS spectra of V 2p core level before (curve a) and after $Li^+$ insertion (curves b & c) at potential 3.2 V and 2.5 V respectively. The increase in the

intensity peak corresponding to $V^{+4}$ is evident in the lithiated samples, D) Low-binding energy valence spectra showing the development of new peak at ~1 eV as a result of $Li^{+}$ insertion.

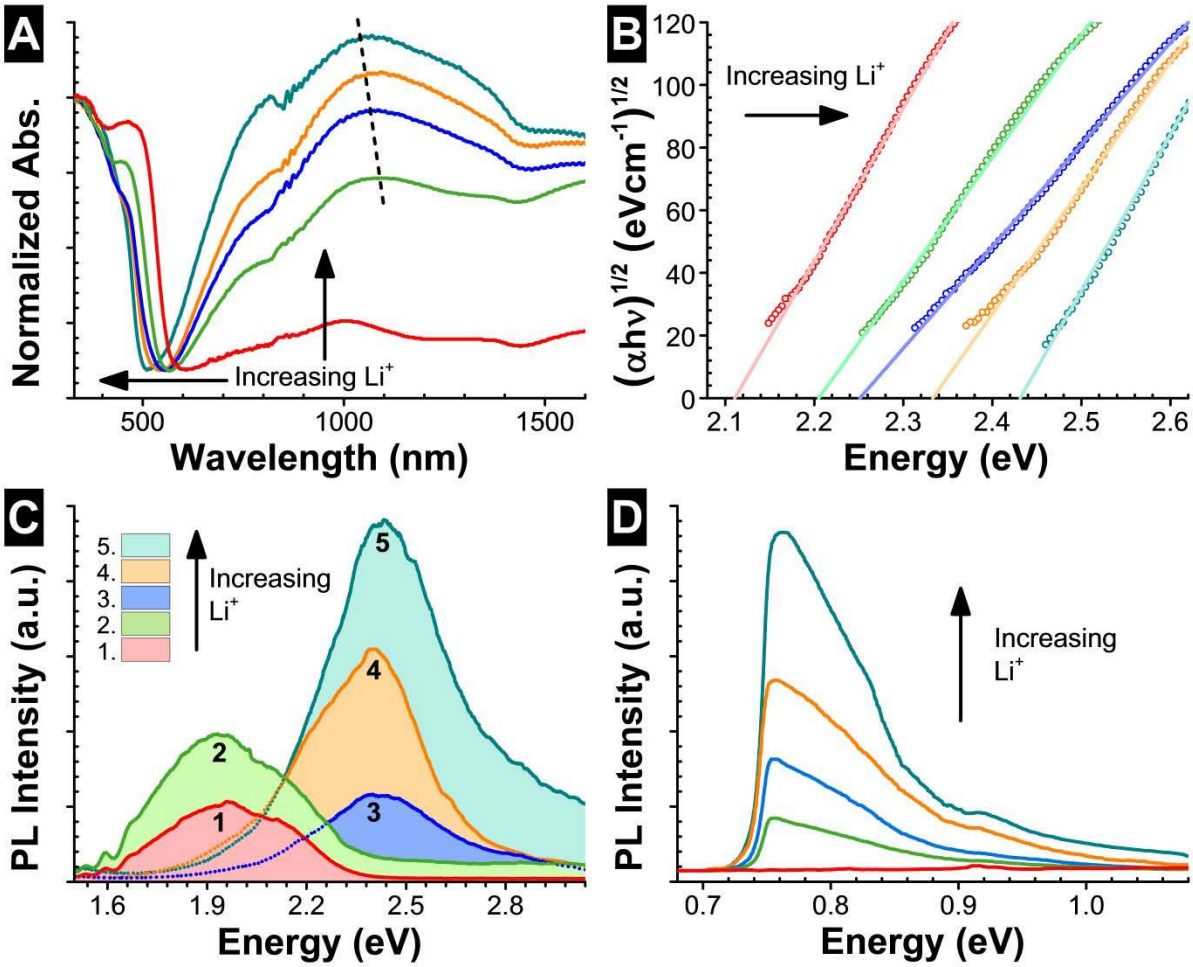


Figure 3. Changes in the optical properties of $V_2O_5$ with increasing concentration of $Li^+$ corresponding to a electrochemical bias of OCP, 3.2 V, 3.0 V, 2.5 V, and 1.5 V vs. $Li/Li^+$, respectively. A) & B) Burstein-Moss shift of the optical absorbance spectra as a result of increasing concentration of $Li^+$ insertion: The blue-shift of the absorption edge from 570 nm to 495 nm (Fig.A), increase in the value of optical band gap from 2.1 to 2.45 eV as estimated from the Tauc plot (Fig.B), and the rise in NIR absorbance peak at ~1200 nm that also shows a small blue-shift of 50 nm with increasing $Li^+$ concentration. The dotted line on the spectra is a guide to the eye, C) Shift in the band-edge PL emission of $V_2O_5$ from 1.95 eV to 2.45 eV with

increasing $Li^+$ concentration in the lattice D) Rise in the intensity of defect-related NIR emission as result of $Li^+$ insertion at various electrochemical potentials.

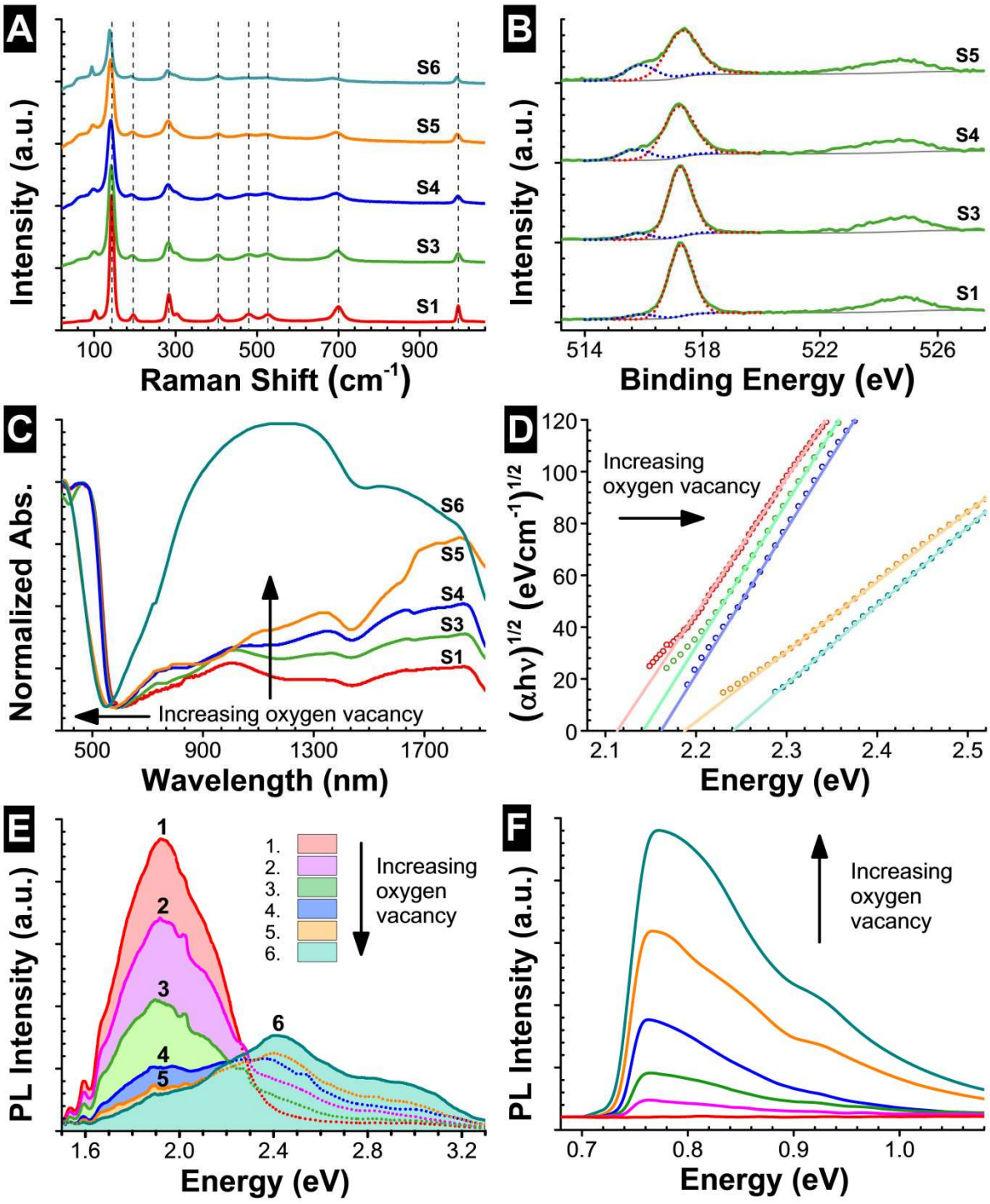


Figure 4 Changes in the composition and optical properties of $V_2O_5$ as result of thermal reduction. A) Raman spectra of oxidized (sample S1) and thermally-reduced phases (samples S3-to-S6) of α-$V_2O_5$, B) Valence band XPS spectra of V 2p core level of oxidized (sample S1)

and thermally-reduced phases (samples S3, S4 and S5), C) Changes in the optical absorbance as a result of increasing oxygen vacancy, $V_O$, defects in the lattice: (i) The blue-shift of the absorption edge from 570 nm to 520 nm (Fig.C) and the value of optical band gap from 2.1 to 2.25 eV, as estimated from the Tauc plot (Fig.D), is a result of Burstein-Moss effect, (ii) Increase in NIR absorbance in the spectral range of 1100-1700 nm, E) Shift in the band-edge PL emission of $V_2O_5$ from 1.95 eV to 2.45 eV with increasing $V_O$ concentration, F) Increase in the intensity of defect-related NIR emission with increasing number of $V_O$ defects. Stoichiometric samples show no NIR emission.

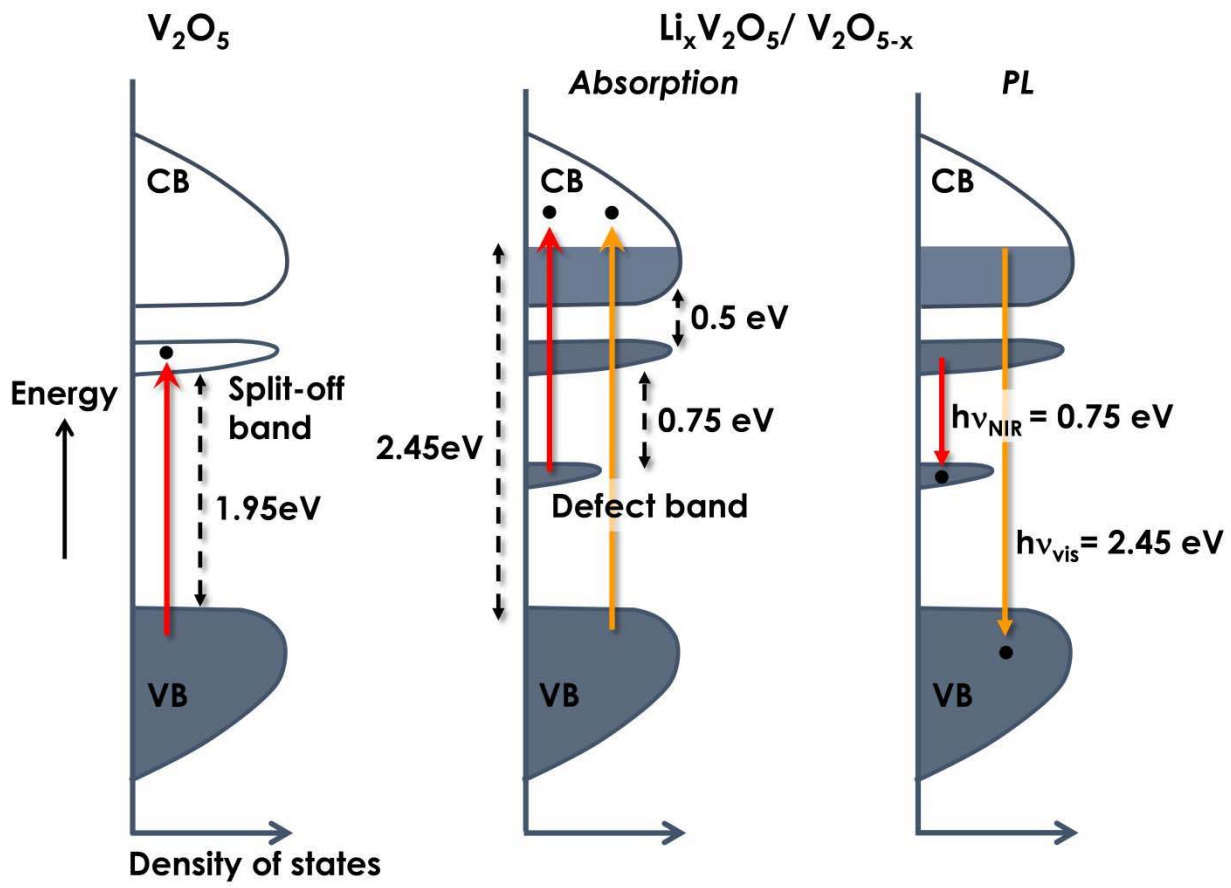


Figure 5: Schematic of the energy band diagrams of $V_2O_5$, $V_2O_{5-x}$ and $Li_xV_2O_5$ showing the mid-gap energy states and the various radiative transitions resulting from the formation of oxygen vacancies for both band gap and sub-band gap excitations. Here, CB and VB refer to conduction and valence band respectively. The defect band refers to mid-gap states resulting from oxygen vacancy defects.

REFERENCES


1. Mamedov, E. A.; Cortés Corberán, V., Oxidative dehydrogenation of lower alkanes on vanadium oxide-based catalysts. The present state of the art and outlooks. *Appl. Cat. A: General* **1995,** *127* (1), 1-40.
2. Mars, P.; van Krevelen, D. W., The Proceedings of the Conference on Oxidation ProcessesOxidations carried out by means of vanadium oxide catalysts. *Chem. Eng. Sci.* **1954,** *3*, 41-59.
3. Amano, F.; Tanaka, T.; Funabiki, T., Steady-State Photocatalytic Epoxidation of Propene by O2 over V2O5/SiO2 Photocatalysts. *Langmuir* **2004,** *20* (10), 4236-4240.
4. Bond, G. C.; Tahir, S. F., Vanadium oxide monolayer catalysts Preparation, characterization and catalytic activity. *Appl. Cat.* **1991,** *71* (1), 1-31.
5. Ji, L.; Lin, Z.; Alcoutlabi, M.; Zhang, X., Recent developments in nanostructured anode materials for rechargeable lithium-ion batteries. *Energy & Environmental Science* **2011,** *4* (8), 2682-2699.
6. Liu, J.; Wang, X.; Peng, Q.; Li, Y., Vanadium Pentoxide Nanobelts: Highly Selective and Stable Ethanol Sensor Materials. *Adv. Mater.* **2005,** *17* (6), 764-767.
7. Yoshitaka, F.; Katsuhiro, M.; Chiei, T., On the Electrochromism of Evaporated V 2 O 5 Films. *Jap. J. Appl. Phys.* **1985,** *24* (8R), 1082.
8. Grzybowska-Świerkosz, B., Vanadia catalysts for selective oxidation of hydrocarbons and their derivativesActive centres on vanadia-based catalysts for selective oxidation of hydrocarbons. *Appl. Cat. A* **1997,** *157* (1), 409-420.

9. Blum, R. P.; Niehus, H.; Hucho, C.; Fortrie, R.; Ganduglia-Pirovano, M. V.; Sauer, J.; Shaikhutdinov, S.; Freund, H. J., Surface Metal-Insulator Transition on a Vanadium Pentoxide (001) Single Crystal. *Phys. Rev. Lett.* **2007,** *99* (22), 226103.

10. Laubach, S.; Schmidt, P. C.; Thi; Fernandez-Madrigal, F. J.; Wu, Q.-H.; Jaegermann, W.; Klemm, M.; Horn, S., Theoretical and experimental determination of the electronic structure of V2O5, reduced V2O5-x and sodium intercalated NaV2O5. *Phys. Chem. Chem. Phys.* **2007,** *9* (20), 2564-2576.

11. Scanlon, D. O.; Walsh, A.; Morgan, B. J.; Watson, G. W., An ab initio Study of Reduction of V2O5 through the Formation of Oxygen Vacancies and Li Intercalation. *J. Phys. Chem. C* **2008,** *112* (26), 9903-9911.

12. Vanhaelst, M.; Clauws, P., EPR Spectrum of the Oxygen Vacancy in Single Crystals V2O5. *Phys. Stat. Sol. B* **1978,** *87* (2), 719-723.

13. Zimmermann, R.; Steiner, P.; Claessen, R.; Reinert, F.; Hüfner, S.; Blaha, P.; Dufek, P., Electronic structure of 3d-transition-metal oxides: on-site Coulomb repulsion versus covalency. *J. Phys. Condens. Matter* **1999,** *11* (7), 1657.

14. Lambrecht, W.; Djafari-Rouhani, B.; Vennik, J., Theoretical study of the vanadyl-oxygen vacancy in V 2 O 5 : tight-binding Green function calculation, optical properties and neutral vacancy ground-state splitting. *J. Phys. C* **1986,** *19* (3), 369.

15. Demeter, M.; Neumann, M.; Reichelt, W., Mixed-valence vanadium oxides studied by XPS. *Surf. Sci.* **2000,** *454–456*, 41-44.

16. Gillis, E.; Boesman, E., E.P.R.-Studies of $V_2O_5$ Single Crystals. I. Defect Centres in Pure, Non-stoichiometric Vanadium Pentoxide. *phys. stat. sol. (b)* **1966,** *14* (2), 337-347.

17. Wu, Q.-H.; Thissen, A.; Jaegermann, W.; Liu, M., Photoelectron spectroscopy study of oxygen vacancy on vanadium oxides surface. *Appl. Surf. Sci* **2004,** *236* (1–4), 473-478.

18. Hermann, K.; Witko; gt; M.; Druzinic, R.; Chakrabarti, A.; Tepper, B.; Elsner, M.; Gorschlüter, A.; Kuhlenbeck, H.; Freund, H. J., Properties and identification of oxygen sites at the V2O5(010) surface: theoretical cluster studies and photoemission experiments. *J. Electron. Spectrosc. Relat. Phenom.* **1999,** *98–99*, 245-256.

19. Ramirez, R.; Casal, B.; Utrera, L.; Ruiz-Hitzky, E., Oxygen reactivity in vanadium pentoxide: electronic structure and infrared spectroscopy studies. *J. Phys. Chem.* **1990,** *94* (26), 8960-8965.

20. Talledo, A.; Granqvist, C. G., Electrochromic vanadium–pentoxide–based films: Structural, electrochemical, and optical properties. *J. Appl. Phys.* **1995,** *77* (9), 4655-4666.

21. Cogan, S. F.; Nguyen, N. M.; Perrotti, S. J.; Rauh, R. D., Optical properties of electrochromic vanadium pentoxide. *J. Appl. Phys.* **1989,** *66* (3), 1333-1337.

22. Wu, Q.-H.; Thißen, A.; Jaegermann, W., Photoelectron spectroscopic study of Li intercalation into V2O5 thin films. *Surf. Sci.* **2005,** *578* (1–3), 203-212.

23. Pecquenard, B.; Gourier, D.; Caurant, D., Electron Nuclear Double Resonance of Polarons in α-$Li_xV_2O_5$. *J. Phys. Chem.* **1996,** *100* (21), 9152-9160.

24. Jiang, J.; Wang, Z.; Chen, L., Structural and Electrochemical Studies on β-LixV2O5 as Cathode Material for Rechargeable Lithium Batteries. *J. Phys. Chem. C* **2007,** *111* (28), 10707-10711.

25. Shin, S.; Tezuka, Y.; Kinoshita, T.; Kakizaki, A.; Ishii, T.; Ueda, Y.; Jang, W.; Takei, H.; Chiba, Y.; Ishigame, M., Observation of local magnetic moments in the Mott transition of $V_6O_{13}$ by photoemission. *Phys. Rev. B* **1992,** *46* (14), 9224-9227.

26. Goschke, R.; Vey, K.; Maier, M.; Walter, U.; Goering, E.; Klemm, M.; Horn, S., Tip induced changes of atomic scale images of the vanadium pentoxide surface. *Surf. Sci.* **1996,** *348* (3), 305-310.

27. Oshio, T.; Sakai, Y.; Ehara, S., Scanning tunneling microscopy/spectroscopy study of $V_2O_5$ surface with oxygen vacancies. *J. Vac. Sci. Tech. B* **1994,** *12* (3), 2055-2059.

28. Pinna, N.; Willinger, M.; Weiss, K.; Urban, J.; Schlögl, R., Local Structure of Nanoscopic Materials: $V_2O_5$ Nanorods and Nanowires. *Nano Lett.* **2003,** *3* (8), 1131-1134.

29. Su, D. S.; Wieske, M.; Beckmann, E.; Blume, A.; Mestl, G.; Schlögl, R., Electron Beam Induced Reduction of $V_2O_5$ Studied by Analytical Electron Microscopy. *Cat. Lett.* **2001,** *75* (1), 81-86.

30. Su, D. S.; Zandbergen, H. W.; Tiemeijer, P. C.; Kothleitner, G.; Hävecker, M.; Hébert, C.; Knop-Gericke, A.; Freitag, B. H.; Hofer, F.; Schlögl, R., High resolution EELS using monochromator and high performance spectrometer: comparison of $V_2O_5$ ELNES with NEXAFS and band structure calculations. *Micron* **2003,** *34* (3–5), 235-238.

31. Wang, Q.; Puntambekar, A.; Chakrapani, V., Vacancy-induced Semiconductor-Insulator-Metal Transitions in Non-Stoichiometric Nickel and Tungsten Oxides. *Nano Lett.* **2016,** *16* (11), 7067–7077.

32. Chakrapani, V.; Brier, M.; Puntambekar, A.; DiGiovanni, T., Modulation of Stoichiometry, Morphology and Composition of Transition Metal Oxide Nanostructures through Hot Wire Chemical Vapor Deposition. *J. Mater. Res. Focus Issue Early Career Scholar in Material Science* **2016,** *31*, 17.

33. Chakrapani, V.; Thangala, J.; Sunkara, M. K., $WO_3$ and $W_2N$ nanowire arrays for photoelectrochemical hydrogen production. *Int. J. Hydrogen Energy* **2009,** *34* (22), 9050-9059.

34. Lide, D. R., *CRC Handbook of Chemistry and Physics*. Chemical Rubber Co. : Boca Raton, 2003.

35. Lambrecht, W.; Djafari-Rouhani, B.; Lannoo, M.; Clauws, P.; Fiermans, L.; Vennik, J., The energy band structure of $V_2O_5$ . II. Analysis of the theoretical results and comparison with experimental data. *J. Phys. C* **1980,** *13* (13), 2503.

36. See Supplemental Material at [] for the changes in Raman, XRD, XPS and optical absorbance spectra before and after thermal and electrochemical reduction of $V_2O_5$.

37. Göbke, D.; Romanyshyn, Y.; Guimond, S.; Sturm, J. M.; Kuhlenbeck, H.; Döbler, J.; Reinhardt, U.; Ganduglia-Pirovano, M. V.; Sauer, J.; Freund, H. J., Formaldehyde formation on vanadium oxide surfaces $V_2O_3$ (0001) and $V_2O_5$ (001): how does the stable methoxy intermediate form? *Angew. Chem. Int. Ed.* **2009,** *48* (20), 3695-3698.

38. Sturm, J. M.; Göbke, D.; Kuhlenbeck, H.; Döbler, J.; Reinhardt, U.; Ganduglia-Pirovano, M. V.; Sauer, J.; Freund, H.-J., Partial oxidation of methanol on well-ordered $V_2O_5$ (001)/Au (111) thin films. *Phys. Chem. Chem. Phys.* **2009,** *11* (17), 3290-3299.

39. Chakrabarti, A.; Hermann, K.; Druzinic, R.; Witko, M.; Wagner, F.; Petersen, M., Geometric and electronic structure of vanadium pentoxide: A density functional bulk and surface study. *Phys. Rev. B* **1999,** *59* (16), 10583-10590.

40. Tepper, B.; Richter, B.; Dupuis, A. C.; Kuhlenbeck, H.; Hucho, C.; Schilbe, P.; bin Yarmo, M. A.; Freund, H. J., Adsorption of molecular and atomic hydrogen on vacuum-cleaved $V_2O_5$ (001). *Surf. Sci.* **2002,** *496* (1–2), 64-72.

41. Lambrecht, W.; Djafari-Rouhani, B.; Vennik, J., Electronic structure of bulk and surface vanadyl oxygen vacancies in the layer compound V2O5. *Surf. Sci.* **1983,** *126* (1), 558-564.

42. Ozkan, U. S.; Cai, Y. P.; Kumthekar, M. W.; Zhang, L. P., Role of Ammonia Oxidation in Selective Catalytic Reduction of Nitric Oxide over Vanadia Catalysts. *J. Catal.* **1993,** *142* (1), 182-197.

43. Calatayud, M.; Minot, C., Reactivity of the Oxygen Sites in the $V_2O_5/TiO_2$ Anatase Catalyst. *J. Phys. Chem. B* **2004,** *108* (40), 15679-15685.

44. Weckhuysen, B. M.; Jehng, J.-M.; Wachs, I. E., In Situ Raman Spectroscopy of Supported Transition Metal Oxide Catalysts: $^{18}O_2$–$^{16}O_2$ Isotopic Labeling Studies. *J. Phys. Chem. B* **2000,** *104* (31), 7382-7387.

45. Lee, E. L.; Wachs, I. E., In Situ Raman Spectroscopy of $SiO_2$-Supported Transition Metal Oxide Catalysts: An Isotopic $^{18}O$–$^{16}O$ Exchange Study. *J. Phys. Chem. C* **2008,** *112* (16), 6487-6498.

46. Xie, S.; Iglesia, E.; Bell, A. T., Effects of Hydration and Dehydration on the Structure of Silica-Supported Vanadia Species. *Langmuir* **2000,** *16* (18), 7162-7167.

47. Muylaert, I.; Van Der Voort, P., Supported vanadium oxide in heterogeneous catalysis: elucidating the structure–activity relationship with spectroscopy. *Phys. Chem. Chem. Phys.* **2009,** *11* (16), 2826-2832.

48. Smirnov, M.; Baddour-Hadjean, R., Li intercalation in $TiO_2$ anatase: Raman spectroscopy and lattice dynamic studies. *J. Chem. Phys.* **2004,** *121* (5), 2348-2355.

49. Banares, M.; Wachs, I., Molecular structures of supported metal oxide catalysts under different environments. *J. Raman Spec.* **2002,** *33* (5), 359-380.

50. Julien, C.; Nazri, G. A.; Bergström, O., Raman Scattering Studies of Microcrystalline $V_6O_{13}$. *phys. stat. sol. (b)* **1997,** *201* (1), 319-326.

51. Baddour-Hadjean, R.; Smirnov, M.; Smirnov, K.; Kazimirov, V. Y.; Gallardo-Amores, J.; Amador, U.; Arroyo-de Dompablo, M.; Pereira-Ramos, J., Lattice dynamics of β-V2O5: Raman spectroscopic insight into the atomistic structure of a high-pressure vanadium pentoxide polymorph. *Inorg. Chem.* **2012,** *51* (5), 3194-3201.

52. Mestl, G.; Ruiz, P.; Delmon, B.; Knozinger, H., Oxygen-Exchange Properties of $MoO_3$: An in situ Raman Spectroscopy Study. *J. Phys. Chem.* **1994,** *98* (44), 11269-11275.

53. Kim, Y. H.; Lee, H.-I., Redox Property of Vanadium Oxide and Its Behavior in Cataltic Oxidation. *Bull. Korean. Chem. Soc.* **1999,** *20* (12), 1457-1463.

54. Smirnov, M. B.; Roginskii, E.; Kazimirov, V. Y.; Smirnov, K. S.; Baddour-Hadjean, R.; Pereira-Ramos, J.-P.; Zhandun, V., Spectroscopic and Computational Study of Structural Changes in γ-$LiV_2O_5$ Cathodic Material Induced by Lithium Intercalation. *J. Phys. Chem. C* **2015,** *119* (36), 20801-20809.

55. Wu, J.; Cao, J.; Han, W. Q.; Janotti, A.; Kim, H. C., *Functional Metal Oxide Nanostructures*. Springer New York: 2011.

56. Poizot, P.; Laruelle, S.; Grugeon, S.; Dupont, L.; Tarascon, J., Nano-sized transition-metal oxides as negative-electrode materials for lithium-ion batteries. *Nature* **2000,** *407* (6803), 496-499.

57. Liu, W.; Huang, X.; Wang, Z.; Li, H.; Chen, L., Studies of Stannic Oxide as an Anode Material for Lithium-Ion Batteries. *J. Electrochem. Soc.* **1998,** *145* (1), 59-62.

58. Lambrecht, W.; Djafari-Rouhani, B.; Vennik, J., On the origin of the split-off conduction bands in V 2 O 5. *J. Phys. C* **1981,** *14* (32), 4785.

59. Bullett, D. W., The energy band structure of $V_2O_5$ : a simpler theoretical approach. *J. Phys. C* **1980,** *13* (23), L595.

60. Naldoni, A.; Allieta, M.; Santangelo, S.; Marelli, M.; Fabbri, F.; Cappelli, S.; Bianchi, C. L.; Psaro, R.; Dal Santo, V., Effect of Nature and Location of Defects on Bandgap Narrowing in Black TiO2 Nanoparticles. *J. Am. Cer. Soc.* **2012,** *134* (18), 7600-7603.

61. Valentí, R.; Saha-Dasgupta, T.; Alvarez, J.; Požgajčić, K.; Gros, C., Modeling the Electronic Behavior of $\gamma-LiV_2O_5$: A Microscopic Study. *Phys. Rev. Lett.* **2001,** *86* (23), 5381.